Chemical Engineering Journal 166 (2011) 138–149

Contents lists available at ScienceDirect

Chemical Engineering Journal

journal homepage: www.elsevier.com/locate/cej

Photocatalytic abatement of VOCs by novel optimized TiO_2 nanoparticles

Murid Hussain[a,b], Nunzio Russo[a,*], Guido Saracco[a]

[a] Department of Materials Science and Chemical Engineering, Politecnico di Torino, Corso Duca degli Abruzzi 24, 10129 Torino, Italy
[b] Department of Chemical Engineering, COMSATS Institute of Information Technology Lahore Campus, M.A. Jinnah Building, Defence Road, Off Raiwind Road, Lahore 54000, Pakistan

ARTICLE INFO

Article history:
Received 27 July 2010
Received in revised form 15 October 2010
Accepted 15 October 2010

Keywords:
TiO_2
Nanoparticles
VOCs
Oxidation
Photocatalysis

ABSTRACT

In this work, photocatalytic degradation of different VOCs has been investigated using novel TiO_2 nanoparticles (TNP) at near room temperature. The TNP was synthesized in a vortex reactor by sol–gel process with controlled operating parameters. The final product was optimized through an effective control of the calcination temperatures (400–700 °C) and times (1–7 h). The optimized 10–20 nm particle size TNPs exposed a high specific surface area (151 m^2/g), which was three times higher than the commercial Degussa P 25 TiO_2 material. It also showed rather pure crystalline anatase with small rutile traces, confined band gap energy, relatively more Ti^{3+} on the surface, and higher OH surface groups as characterized by X-ray diffraction (XRD), Raman spectroscopy, specific surface area analysis, diffuse reflectance ultraviolet–visible spectroscopy (DR/UV–vis), Fourier transformed-infrared spectroscopy (FT-IR) and X-ray photoelectron spectroscopy (XPS). The optimized TNP showed superior photocatalytic degradation of ethylene at ambient temperature, as tested in an ad hoc designed Pyrex glass photocatalytic reactor. It was found that the mixed phase of the optimized TNP with a high surface area might induce the adsorption of ethylene and water and generate OH groups which act as oxidizing agents on the TNPs surface, leading to higher photocatalytic activity. The effects of different factors, including adsorption, flow rates, concentrations, catalyst weight and reaction temperature were studied in detail for ethylene, propylene, and toluene oxidation. Moreover, higher photocatalytic activity for VOCs abatement was obtained than the Degussa P 25 TiO_2 due to the above-mentioned characteristics.

1. Introduction

Volatile organic compounds (VOCs) are considered to be as some of the most important anthropogenic pollutants generated in urban and industrial areas [1]. These VOCs are widely used in (and produced by) both industrial and domestic activities since they are ubiquitous chemicals that are used as industrial cleaning and degreasing solvents [2]. VOCs come from many well-known indoor sources, including cooking and tobacco smoke, building materials, furnishings, dry cleaning agents, paints, glues, cosmetics, textiles, plastics, polishes, disinfectants, household insecticides, and combustion sources [2–4].

Many VOCs are toxic, and some are considered to be carcinogenic, mutagenic, or teratogenic [5–7]. Carcinogen VOCs have no safety threshold dose, thus any exposure, however small, implies a finite risk. Long-term exposure to these VOCs is detrimental to human health (sick building syndrome, SBS). Furthermore, VOC emissions can contribute to the formation of urban smog and ozone, stratospheric ozone depletion and the greenhouse effect.

New, safe, and clean chemical technologies and processes for VOC abatement are currently under development [8]. Conventionally, VOC pollutants are removed by air purifiers that employ filters to remove particulate matters or use sorption materials (e.g. granular activated carbon) to adsorb the VOC molecules [9]. These techniques only transfer the contaminants to another phase instead of destroying them. Hence, additional disposal or handling steps are needed. Moreover, all these sequestration techniques have inherent limitations, and none of them is decisively cost effective. Therefore, there is a great demand for a more cost effective and environmentally benign process that is capable of eliminating VOCs from gas streams [10], such as photochemical degradation, UV photolysis and photo-oxidation in the presence of some oxidants such as ozone. Photocatalytic oxidation (PCO) of VOCs is a very attractive and promising alternative technology for air purification [11,12]. It has been demonstrated that organics can be oxidized to carbon dioxide, water and simple mineral acids at low temperatures on TiO_2 catalysts in the presence of UV or near-UV illumination. PCO requires a low temperature and pressure, employs inexpensive semiconducting catalysts, and is suitable for the oxidation of a wide range of organics. Researchers [11–25] have already focused on this promising technique and many beneficial advancements have been

* Corresponding author. Tel.: +39 011 0904710; fax: +39 011 5644699.
E-mail address: nunzio.russo@polito.it (N. Russo).

1385-8947/$ – see front matter © 2010 Elsevier B.V. All rights reserved.
doi:10.1016/j.cej.2010.10.040

made in the field of VOC abatement. The performance of the semiconducting photocatalyst depends mainly on its nature and morphology.

Solids that can promote reactions in the presence of light and which are not consumed in the overall reaction are referred to as photocatalysts [26]. These are invariably semiconductors. A good photocatalyst should be photoactive, able to utilize visible and/or near UV light, biologically and chemically inert, photostable, inexpensive and non-toxic. For a semiconductor to be photochemically active as a sensitizer for the aforementioned reaction, the redox potential of the photogenerated valence band hole should be sufficiently positive to generate $OH^{\bullet}$ radicals that can subsequently oxidize the organic pollutant. The redox potential of the photogenerated conductance band electron must be sufficiently negative to be able to reduce the adsorbed O_2 to a superoxide. TiO_2, ZnO, WO_3, CdS, ZnS, $SrTiO_3$, SnO_2 and Fe_2O_3 can be used as photocatalysts.

TiO_2 is an ideal photocatalyst for several reasons [26–33]. It is relatively cheap, highly stable from a chemical point of view and easily available. Moreover, its photogenerated holes are highly oxidizing, and the photogenerated electrons are sufficiently reducing to produce superoxides from dioxygen groups. TiO_2 promotes ambient temperature oxidation of most indoor air pollutants and does not need any chemical additives. It has also been widely accepted and exploited as an efficient technology to kill bacteria.

Most of the studies have shown that the photocatalytic activity of titanium dioxide is influenced to a great extent by the crystalline form, although controversial results have also been reported in the literature. Some authors have stated that anatase works better than rutile [22], others have found the best photocatalytic activity for rutile [34], and some others have detected synergistic effects in the photocatalytic activity for anatase–rutile mixed phases [35]. It has recently been demonstrated that photo-activity towards organic degradation depends on the phase composition and on the oxidizing agent; for example, when the performance of different crystalline forms was compared, it was discovered that rutile shows the highest photocatalytic activity with H_2O_2, whereas anatase shows the highest with O_2 [36]. Moreover, the ability of titanium dioxide particles to degrade organic compounds also depends on the size of the particles, since small particles offer larger specific surface areas [37]. It has also been found that photoformed OH species, as well as O_2^- and O_3^- anion radicals, play a significant role as a key active species in the complete photocatalytic oxidation of ethylene with oxygen into carbon dioxide and water [11].

In our previous work [25], we focused in particular on the synthesis of TNPs at a large scale by controlling the optimized operating conditions and using a special passive mixer, i.e. a vortex reactor (VR). An attempt was made to obtain TNPs with a high surface area and a mixed crystalline phase with more anatase and small amounts of rutile, and it was found to guarantee good photocatalytic activity.

Instead, in the present work, an attempt has been made to optimize TNPs catalyst by optimizing the synthesis operating conditions. The optimized TNPs were then tested for the photocatalytic oxidation of several key pollutants: ethylene (generated by engines, biomass fermentators, pyrolysis of hydrocarbons, fruit ripening, and plants biosynthesis), propylene (produced from non-renewable fossil fuels, natural gas processing, coal, oil refining), and toluene (emitted by refining processes, paints, thinners, adhesives, nail polish, automobile exhausts, cosmetics, rubber, cement, fabric dyes, inks). Various operating conditions, including adsorption, specific flow rate, pollutant concentrations, catalyst weight, and reaction temperature have been studied in detail for ethylene, propylene, and toluene VOC abatement. The materials were characterized through X-ray diffraction (XRD), Raman spectroscopy, specific surface area analysis, diffuse reflectance ultraviolet–visible spectroscopy (DR/UV–vis), Fourier transformed-infrared spectroscopy (FT-IR) and X-ray photoelectron spectroscopy (XPS) in order to analyze the reaction mechanism. The photocatalytic activity of the optimized TNP was then compared with that of commercially purchased Degussa P 25 TiO_2.

2. Experimental

2.1. Synthesis of the TNP photocatalysts

The TNPs were synthesized at a large scale (2 L gel) by controlling the optimized operating parameters using the VR according to our previous work [25]. Titanium tetra-isopropoxide (TTIP: Sigma–Aldrich) was used as a precursor in this synthesis, because of its very rapid hydrolysis kinetics. Two solutions, one of TTIP in isopropyl alcohol and the other of water (Milli-Q) in isopropyl alcohol, were prepared separately under nitrogen flux to control the alkoxide reactivity with humidity. Hydrochloric acid (HCl: Sigma–Aldrich) was added to the second solution as a hydrolysis catalyst and deagglomeration agent. A TTIP/isopropanol concentration was taken as 1 M/L to obtain the maximum TiO_2 yield (1 M), W ($[H_2O]/[TTIP]$) = 4, whereas for H the $[H^+]/[TTIP]$ ratio was set to 0.5. The two TTIP and water in isopropyl alcohol solutions were stored in two identical vessels, then pressurized, at 2 bar, with analytical grade nitrogen at inlet flow rates of 100 mL/min with two rota meters and were mixed in the VR. Equal volumes of reactant solutions (i.e., 1 L) were mixed at equal flow rates at 28 °C and then for both configurations the solutions exiting from the VR were collected in a beaker thermostated at 28 °C and gently stirred.

The mixed solutions (i.e. gel) were then dried using a rotary evaporator. Complete drying was obtained at 150 °C overnight. The resulting dried powders were eventually calcined at different calcination temperatures of 400, 500, 600 and 700 °C for 3 h in order to screen the optimized calcination temperature. The dried samples were also calcined at different calcination times of 1, 3, 5, and 7 h at 400 °C to highlight the effect of calcination time. The Degussa P 25 TiO_2 was purchased from Aerosil.

2.2. Characterization of the TNP photocatalysts

The XRD patterns were recorded to determine the different polymorphs, on an X'Pert Phillips diffractomer using Cu Kα radiation, under the following conditions: 2θ = 10–90; 2θ step size = 0.02. The Raman spectra were measured by means of a Renishaw Ramanscope with a green laser (Ar+, 514 nm), a notch filter, lenses, a spectrograph and a CCD detector. The BET specific surface area measurement was carried out on powders previously outgassed, at 150 °C, by means of N_2 sorption at 77 K on a Quantachrome Autosorbe 1 C instrument. The DR/UV–vis spectroscopy was accomplished using a UV–vis double beam spectrophotometer Varian Cary 500. The reference for background subtraction was Spectralon® and the spectra were collected in 200–600 nm regions with a resolution of 2 nm. CO_2 and CO were measured by carbon analyzer (AO 2000 Series; ABB Automation Products Germany) at the outlet of the reactor.

VOC adsorption experiments were performed at 25 °C for 220 min in a Pyrex glass reactor. 0.1 g TNP sample was used for the adsorption of ethylene/propylene/toluene at 200 ppm concentration and 100 mL/min flow rate. The adsorption runs were carried out under continuous flow for about 220 min, a time that was in any case sufficient to saturate the TNP sample. The overall equilibrium amount of adsorbed hydrocarbons could be estimated from the related breakthrough curves.

Information about the nature of the surface groups on titania was obtained through FT-IR spectroscopy. The powders

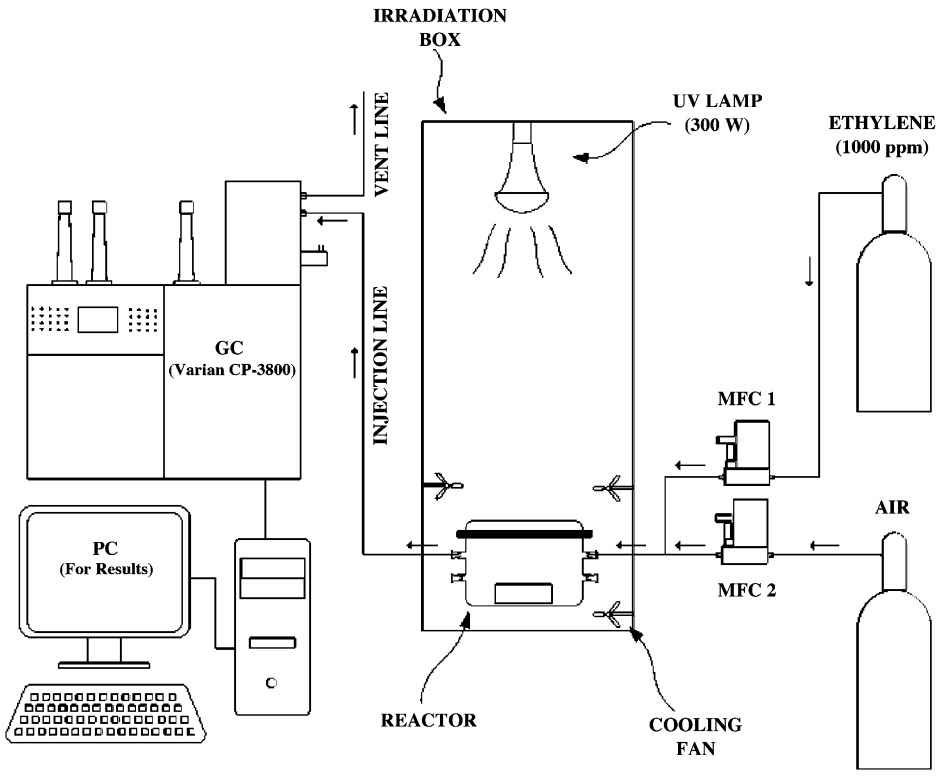

Fig. 1. Schematic photocatalytic reaction experimental set up.

were pressed into thin, self-supporting wafers. The spectra were collected, at a resolution of 2 cm^{-1}, on a PerkinElmer FT-IR spectrophotometer equipped with an MCT detector. The XPS spectra were recorded using a PHI 5000 Versa Probe with a scanning ESCA microscope fitted with an X-ray source of Al monochromatic (1486.6 eV, 25.6 W), a beam diameter of 100 μm, a neutralizer at 1.4 eV 20 mA, and a FAT analyzer mode. All the binding energies were referenced to the C 1s peak at 284 eV of the surface adventious carbon. The individual components were obtained by curve fitting after proper subtraction of the baseline.

2.3. VOC photocatalytic oxidation tests

All the ethylene, propylene, and toluene photocatalytic degradation test were performed in a Pyrex glass reactor with a total volume of 2 L. A schematic of the photocatalysis reaction experimental setup has been shown in Fig. 1. The setup includes a Pyrex glass reactor (transparent to UV light), connectors, mass flow controllers (MFC, Bronkhorst high tech), a UV lamp (Osram ULTRA-VITALUX 300 W; has a mixture of light of UVA ranging 320–400 nm and UVB with 290–320 nm wavelength which produces 13.6 and 3.0 W radiations, respectively; is ozone-free and radiations are produced by a mixture of quartz burner and a tungsten wire filament, as provided in manufacturer's informations), gas cylinders (1000 ppm ethylene/propylene/toluene), and a gas chromatograph (Varian CP-3800) equipped with a capillary column (CP7381) and a flame ionization detector (FID) with a patented ceramic flame tip for ultimate peak shape and sensitivity, which was used for the products gas analysis.

The calcined TiO_2 photocatalyst sample was spread homogeneously through hands inside the Pyrex glass reactor. An initial humidity of 60% was provided to the photocatalyst to initiate the photocatalytic reaction. The VOC (ethylene or propylene or toluene) was continuously flushed in the reactor, with the help of the MFC, at a constant flow rate of 100 mL/min. After achieving equilibrium in the peak intensity, the UV light was turned on, the reaction products were analyzed by GC, and the conversion was eventually calculated. The reaction experiments were repeated twice and the results had shown reproducibility.

3. Results and discussion

3.1. Characterization and optimization of the TNP photocatalyst

Fig. 2a shows the effect of calcination temperatures at specific moderate calcination time (3 h) on the TNP by XRD patterns in order to screen the optimized calcination temperature. It was found that when the calcination temperature was below 500 °C, the TNP sample dominantly displayed the anatase phase with just small amounts of rutile. The Raman spectroscopy (Fig. 3) supported the XRD results by showing the anatase phase peaks at 395, 513, and 639 cm^{-1} and the rutile peak at 447 cm^{-1} [33]. When the calcination temperature was increased to 600 °C, the anatase to rutile phase transformation gets accelerated as shown by the transition peak of the Raman spectra in Fig. 3 which indicates the Raman shift. A further increase in the calcination temperature to 700 °C resulted in the clear transformation of anatase into rutile, as demonstrated by the growth in the XRD rutile peaks (R) in Fig. 2a. The synthesized TNP was dried in a rotary evaporator and this was followed by complete water evaporation at 150 °C in the oven before calcination. Just after drying, the powder was mainly amorphous and no distinct peak was found, as shown in Fig. 2b, except very low intensity peaks at $2\theta = 38.47$, 44.7, 65.0 and 78.2, which are due to the aluminum sample holder. These aluminum sample holder peaks are also dominantly observed in other samples as shown in Fig. 2. The effect of calcination times on the characteristics of TNP is shown in Fig. 2b; these data indicate that even the longer calcination time (7 h) has no significant effect on the TNP and the main phase remain anatase with minor rutile. Therefore, the effect of calcination times at 400 °C is not so

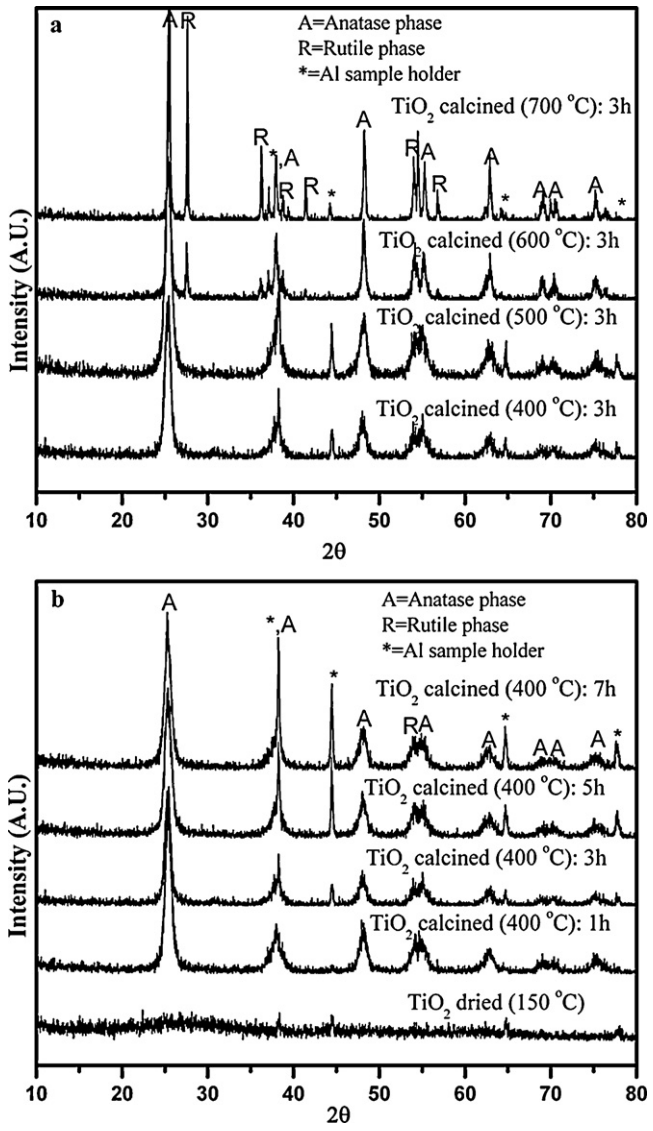

Fig. 2. XRD patterns of TNP at different calcination (a) temperatures and (b) times.

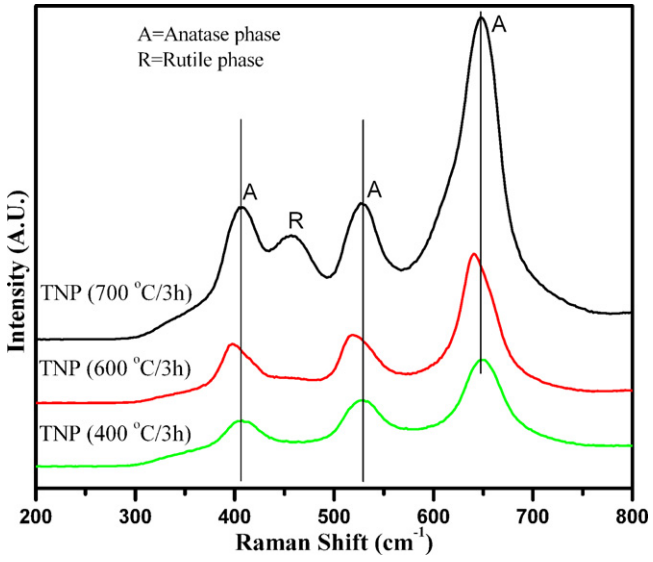

Fig. 3. Raman spectra of TNP calcined at different temperatures.

Table 1
Calcination temperature and time effect on BET surface area analysis of TNP.

Calcination temperature effect		Calcination time effect	
Sample	S_{BET} (m^2/g)	Sample	S_{BET} (m^2/g)
TNP (400 °C/3 h)	151	TNP (400 °C/1 h)	109
TNP (500 °C/3 h)	140	TNP (400 °C/3 h)	151
TNP (600 °C/3 h)	26	TNP (400 °C/5 h)	130
TNP (700 °C/3 h)	3	TNP (400 °C/7 h)	127

severe.

It is generally accepted that anatase demonstrates a higher activity than rutile, for most photocatalytic reaction systems, and this enhancement in photoactivity has been ascribed to the fact that the Fermi level of anatase is higher than that of rutile [38]. The precursors and the preparation method both affect the physicochemical properties of the specimen. In recent years, Degussa P 25 TiO_2 has set the standard for photoreactivity in environmental VOC applications. Degussa P 25 is a non-porous 70:30% (anatase to rutile) material. Despite the presence of the rutile phase, this material has proved to be even more reactive than pure anatase [26]. Therefore, a mixed anatase–rutile phase seems to be preferable to enable some synergistic effects for photocatalytic reactions since the conduction band electron of the anatase partly jumps to the less positive rutile part, thus reducing the recombination rate of the electrons and positive holes in the anatase part. The synthesized TNP is actually characterized by the similar anatase–rutile mixture.

The effect of the specific surface area of TiO_2 in photocatalysis is always important [26]. The primary objective was to synthesize the TNPs with the highest possible surface area [25]. Table 1 shows all the specific surface areas of TNP samples at different calcination temperatures and times. The results of the calcination temperature effect entailed a more severe decrease in the BET surface area, as shown in Table 1. Calcination at 700 °C entailed a very low surface area of 3 m^2/g. This decrease in surface might be related to the increased amount of rutile. Hence the BET results seem to be consistent with the XRD and Raman findings. However, the TNP sample calcined at 400 °C for 3 h showed an optimized higher BET surface area that was 3 times higher than that of the reference Degussa P 25 material (53 m^2/g). TNP also shows a good porosity with a pore volume of 0.20 cm^3/g and an average pore diameter of 7 nm [25] which favors a high adsorptive capacity. Moreover, the increased surface area of TiO_2 should be helpful to enhance the surface reaction. An increase in calcination time from 1 to 3 h increased the BET surface area as a likely consequence of a loss of impurities and water molecules, but a further increase of 5–7 h caused a gradual decrease.

Fig. 4a and b and Table 2 show the UV–vis absorption profiles of TNP at different calcination temperatures and times. The DR/UV–vis spectroscopy provides some insight into the interactions of the photocatalytic materials (e.g. TiO_2) with photon energies [33,38]. It is clear that the absorption spectrum of TNP calcined at different calcination temperatures exhibits the onset of absorption at $\lambda = 391$, 396, and 422 whereas calcination times at $\lambda = 395$, 391, 393, and 398 nm, exhibit the more intensive effect of temperature and the less prominent effect of time on the evolution of the crystalline structure. After the impurities and water molecules had left the sample, a gradual decrease and shift in the absorption peaks was observed due to the increased calcination temperatures and times. The band gap energy of the titania samples was calculated using these UV–vis DRS spectra values with the equation, $E(eV) = hc/\lambda = 1239.95/\lambda$ [33], where E is the band gap energy (eV), h is Planck's constant, c is the velocity of light (m/s) and λ is the wavelength in nm. Table 2 shows the calculated band gap energies and the comparison. The average literature values for the absorption and the corresponding band gap energies for bulk anatase TiO_2 are

Table 2
Effect of calcination temperature and time of TNP on band gap energy.

Calcination temperature effect			Calcination time effect		
Sample	Absorption edge wave length, λ (nm)	Band gap energy, *E* (eV)	Sample	Absorption edge wave length, λ (nm)	Band gap energy, *E* (eV)
400 °C/3 h	391	3.17	400 °C/1 h	395	3.14
600 °C/3 h	396	3.13	400 °C/3 h	391	3.17
700 °C/3 h	422	2.94	400 °C/5 h	393	3.16
			400 °C/7 h	398	3.12

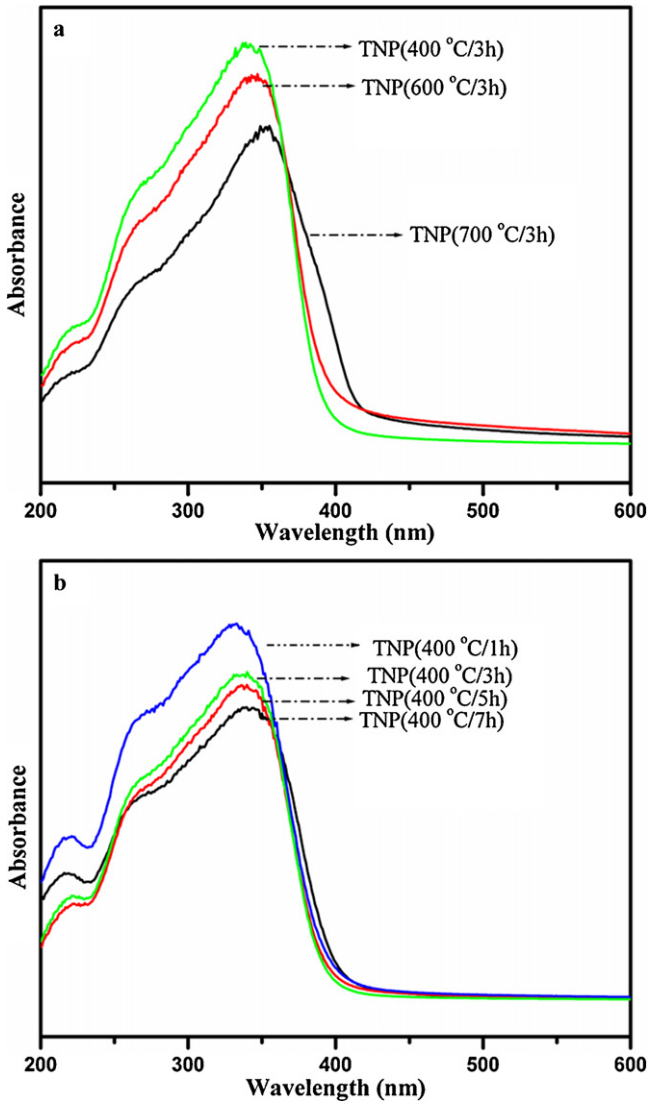

Fig. 4. DR/UV–vis spectra of TNP at different calcination (a) temperatures and (b) times showing the difference in wavelength.

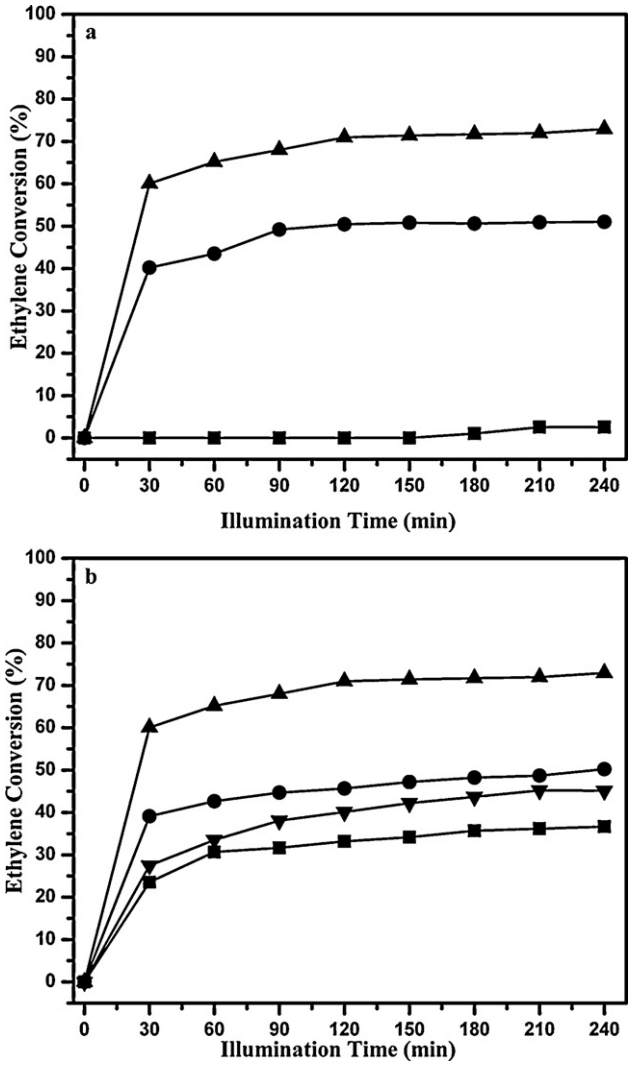

Fig. 5. Ethylene oxidation over TNP photocatalysts at different calcination (a) temperatures: (▲) 400 °C/3 h; (●) 600 °C/3 h; (■) 700 °C/3 h and (b) times: (▼) 400 °C/1 h; (▲) 400 °C/3 h; (●) 400 °C/5 h; (■) 400 °C/7 h. *Operating conditions*: feed concentration = 200 ppm; flow rate = 100 mL/min, room temperature; 1 g of TNP catalyst.

λ_{on} 385 nm and E = 3.2 eV [39] whereas these are λ_{on} 413 nm and E = 3.0 eV for rutile TiO_2 [30]. Therefore, from Table 2 it is clear that all the presented data are reasonably in line with expectations and that the higher calcination temperatures and times have increased the rutile phase since the overall binding energies have decreased.

3.2. Ethylene photocatalytic degradation over the TNP photocatalyst

The PCO of ethylene was performed at ambient temperature over TNP calcined at different calcination temperatures and times (Fig. 5) in order to check the catalytic performance of the developed TNP material. Air was used instead of conventional oxygen to get data more representative for practical application conditions, leading towards commercialization. After a preliminary saturation of the sample under an ethylene flow, there was no conversion in the dark in any of the experiments even in the presence of catalyst or in the presence of UV light and the absence of catalyst. Therefore, it can be concluded that the reaction results reported hereafter are only photocatalytically induced. Fig. 5a and b shows the percentage conversion of ethylene as a function of illumination time. A steady-state conversion is reached after approximately 6 h of illumination time for all the samples. This rather long time is required for the experimental apparatus employed, on the one hand because

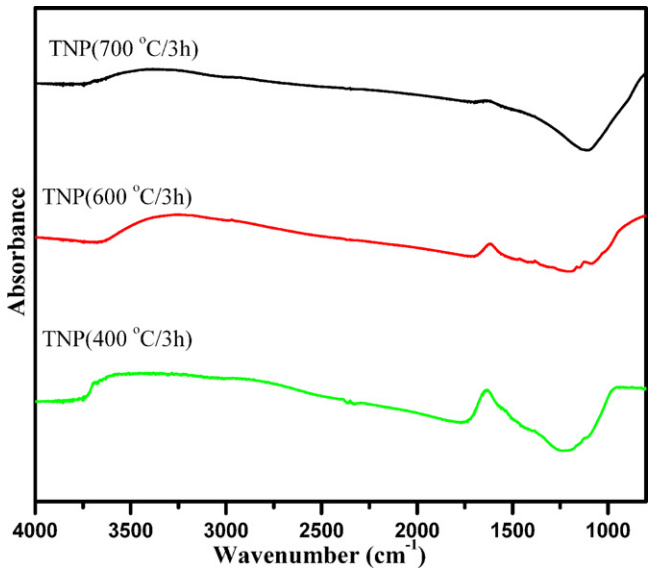

Fig. 6. FT-IR spectra of TNP samples calcined at different temperatures showing the comparison of OH groups.

of fluid-dynamic reasons and on the other hand to get the surface of the sample at a steady, equilibrium coverage value. The CO and CO_2 measurements of the outlet gases demonstrated that ethylene completely oxidizes to CO_2 with just traces of CO.

The highest calcination temperature (700 °C) TNP sample showed the worst performance as shown in Fig. 5a. However, the highest conversion was obtained for TNP calcined at 400 °C for 3 h. As expected, all other sample preparation conditions resulted in a lower catalytic activity. In other words, at the highest calcination time (7 h), the TNP sample also showed the lowest activity, as shown in Fig. 5b. These reaction results of TNP calcined at different calcination temperatures and times are in perfect agreement with their characterization results of the XRD, Raman, UV–vis, and BET analyses. The TNP sample calcined at 400 °C for 3 h proved to be the best performing one of all the samples. As previously mentioned, it possesses superior characteristics of the mixed anatase (80%)–rutile(20%) phase, confined band gap energy of 3.17 eV, and the highest BET specific surface area, of 151 m^2/g, compared to all the others and therefore showed the best catalytic performance.

3.3. Influence of the hydroxyl groups on the optimized TNP photocatalyst

It has been observed that the surface OH groups and/or physisorbed H_2O, as well as the anion radicals, can play a significant role as key active species in the photocatalytic oxidation reaction of various VOCs [8,11,14,27,29,40–45]. It has been stated that the presence of water (or humid air) or/and OH• radicals (second best universal oxidant) leads easily to total oxidation. Fig. 6 shows the FT-IR spectra of TNP calcined at three different temperatures in order to analyze the status of the surface OH groups. The broad peak centered at 3400 and the peak at 1650 cm^{-1} correspond to the surface adsorbed water and hydroxyl groups. The optimized TNP calcined at 400 °C/3 h with a high surface area has in fact shown higher bands at 3400 and 1650 cm^{-1}, and this should be responsible for its higher activity. As the calcination temperature increase, these hydroxyl groups decrease significantly as a consequence of the low surface area exposed and of surface dehydration.

3.4. The optimized TNP photocatalytic mechanism for ethylene degradation

On the basis of the literature, the first main step should be the adsorption of water, O_2, and ethylene on the surface of TNP followed by the formation of hole–electron pairs which need sufficient energy to overcome the band gap between the valence band (VB) and the conduction band (CB) [2]. The TNP catalyst derives its activity from the fact that when photons of a certain wavelength hit its surface, electrons are promoted from the valence band and transferred to the conductance band. This leaves positive holes in the valence band, which then reacts with the hydroxylated surface to produce OH• radicals, the true oxidizing agents. In the absence of suitable electron and hole scavengers, the stored energy is dissipated in a few nanoseconds through recombination. If a suitable scavenger or a surface defect state is available to trap the electron or hole, their recombination is prevented and a subsequent redox reaction may occur [26]. The synergistic effect of the anatase–rutile mixed phase in the TNP material which is similar to the Degussa P 25 one, acts a scavenger. The conduction band electron of the anatase part jumps to the less positive rutile part, reducing the recombination rate of the electrons and positive holes in the anatase part. These •OH and $•O_2^-$ which are produced as shown in Eqs. (2)–(4), further react with ethylene to produce CO_2 and water, as represented in Eqs. (5) and (6).

$$TiO_2 + h\nu \rightarrow h^+(VB) + e^-(CB) \quad (1)$$

$$H_2O + h^+(VB) \rightarrow OH^- + H^+ \quad (2)$$

$$h^+(VB) + OH^- \rightarrow •OH \quad (3)$$

$$O_2 + e^-(CB) \rightarrow •O_2^- \quad (4)$$

$$•OH + C_2H_4 \rightarrow (C_2H_4OH)* \quad (5)$$

$$(C_2H_4OH)* + •O_2 \rightarrow CO_2 + H_2O \quad (6)$$

$$Ti(IV) + e^- \rightarrow Ti(III) \quad (7)$$

$$Ti(III) + O_2 \rightarrow Ti(IV) + O_2^- \quad (8)$$

3.5. Factors that affect the optimized TNP for the photocatalytic abatement of different VOCs

After optimization of the TNP, the PCO of three VOCs, two alkenes (ethylene, propylene) and one aromatic substance (toluene) was carried out. The PCO of the VOCs by TiO_2 is affected by several factors, including the adsorption of the pollutant, the concentration, the flow rate, the humidity, the UV light, and the catalyst weight [9,16,18,23]. In this section, some of the important factors are discussed for ethylene, propylene, and toluene PCO over the optimized TNP.

3.5.1. Adsorption and flow rate effect

Adsorption of pollutants on the titania surface is one of the most important parameter the catalyst performance. The adsorption trends of these pollutants may determine their conversion rate. As shown in Fig. 7, ethylene undergoes a lower adsorption phenomenon compared to the other hydrocarbons tested, whereas propylene has slightly higher adsorption than ethylene on the optimized TNP surface. Compared to both ethylene and propylene, toluene has very high adsorption which might be due to its larger size. Total areas above the adsorption curves of ethylene, propylene and toluene and the saturation line were calculated from Fig. 7. The relative size is 1:1.25:7.24, respectively. Based on further calculations it could be ascertained that the minimum required TNP specific surface area for total ethylene adsorption is 0.815 m^2/g. However, the specific surface area of TNP available with the 0.1 g

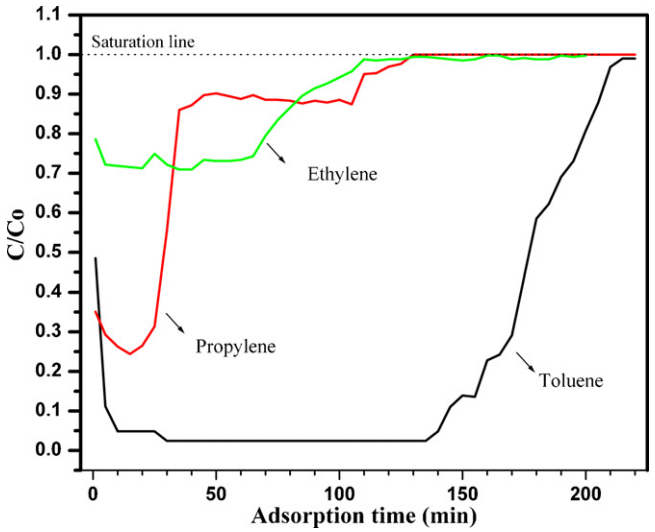

Fig. 7. Adsorption of ethylene, propylene and toluene at optimized TNP photocatalyst.

used in the experiment is 15 m^2/g. Therefore, ethylene undergoes quite likely a monolayer adsorption. Similarly, for propylene, specific surface area required is 1.53 m^2/g whereas the available one is 15 m^2/g, which also entails a monolayer adsorption. Conversely, for toluene, the required surface area for the total adsorbed amount detected is 19.425 m^2/g which exceeds the available 15 m^2/g. This shows that toluene undergoes multilayer adsorption under the tested conditions.

The first important factor is the feed flow rate of pollutants in the reactor. Fig. 8 shows the effect of the flow rate on ethylene (Fig. 8a), propylene (Fig. 8b), and toluene (Fig. 8c). As shown in Fig. 8a, the steady-state ethylene conversion decreased as the flow rate increased from 100 to 300 mL/min. The peak in ethylene conversion observed after 30 min for the higher feed flow rates should be ascribed to the fact that, at the beginning of the runs, the surface coverage of ethylene is maximized by the preliminary saturation treatment. This enhances the initial conversion rate which then progressively becomes tuned to lower values as the surface coverage reaches its steady-state values. CO_2 measurements at the reactor outlet provided concentration values those were compatible with complete oxidation.

In the case of propylene (Fig. 8b), a similar decreasing conversion trend was found along with the increase in the flow rate. Higher flow rates than 300 mL/min significantly decreased the conversion as compared to 100 mL/min. Initially, the propylene conversion was high, but as the irradiation time passed, deactivation was observed. The carbon balance evaluation based on the CO and CO_2 measurements at the reactor outlet, would seem to suggest that byproducts are formed which may further polymerize or adsorb onto the surface and cause deactivation. This deactivation behavior of propylene was further confirmed by FT-IR analysis shown in Fig. 9. The spectrum for TNP after reaction with propylene is entirely different than ethylene in the region 2900–3800 cm^{-1}. Region 2900 cm^{-1} shows the formation of polyethylene/polypropylene as possible byproducts. However, in case of propylene spectrum, OH associated carboxylic acids were observed in the region 3000–3400 cm^{-1} which consumed the OH groups of TNP that caused the main deactivation. Similarly the OH groups at 1650 cm^{-1} were also reduced after reaction.

A similar flow rate-conversion trend was noticed in toluene degradation, but with a much lower conversion and deactivation at higher flow rates. Moreover, the toluene conversion trend with the illumination time increased gradually. This could be due to the

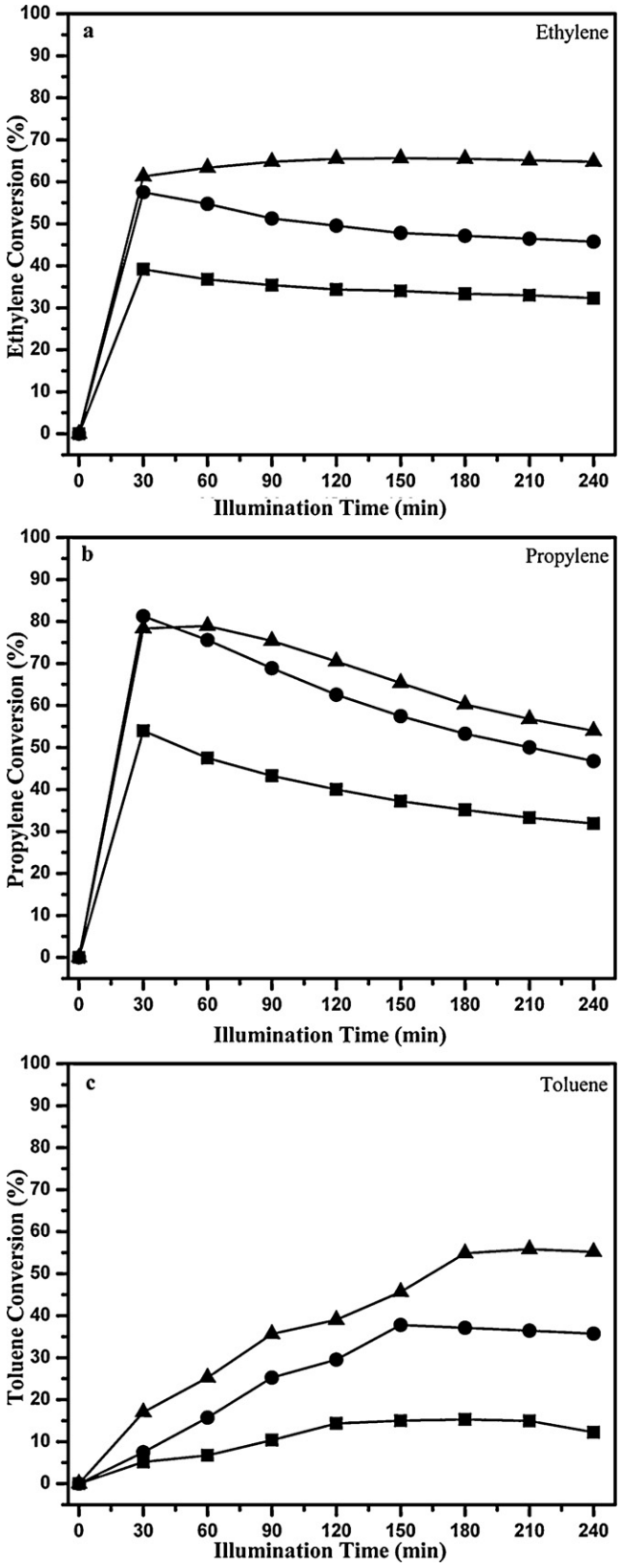

Fig. 8. Effect of flow rate on the photocatalytic activity of the optimized TNP for VOCs abatement (a) ethylene, (b) propylene, (c) toluene, fed at 200 ppm, at room temperature, over 1 g of TNP (400 °C/3 h): (▲) 100 mL/min; (●) 200 mL/min; (■) 300 mL/min.

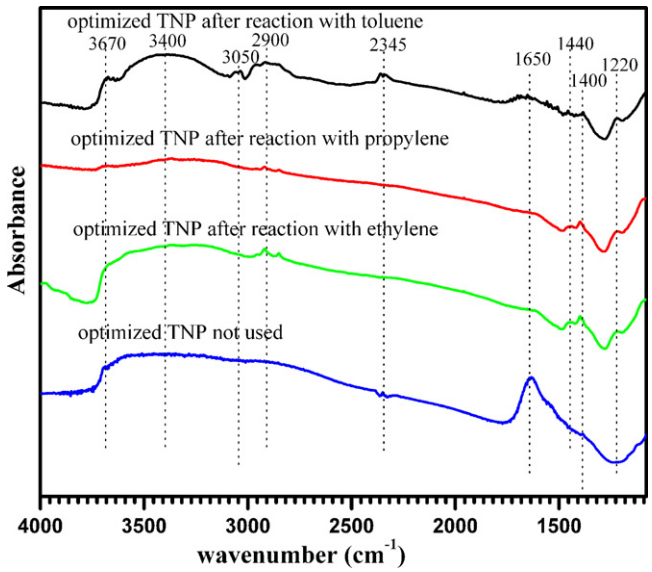

Fig. 9. FT-IR spectra of optimized TNP after reaction with ethylene, propylene and toluene.

slow reaction of toluene with TiO_2, compared to ethylene or propylene. It could also be due to the higher adsorption of toluene (Fig. 7) in the form of multilayers on the surface of the TNP, in part due to its higher molecular weight. Therefore, the reaction at the beginning might be slow due to the surface flooding of the TNP with the heavy toluene and it gets accelerated with the passing of time as toluene reacts, making larger and larger fractions of surface available for further reaction. In general, when the flow rate increases, two antagonistic effects are brought into play: the decrease in residence time within the photocatalytic reactor and the increase in the mass transfer rate [9,16,18]. In this case, a too high flow rate caused the shorter residence time, which eventually reduced the degradation amount of the pollutant. Although the too high flow rate resulted in a shorter residence time, it also increased the convective mass transfer between the pollutant and optimized TNP. This has proved that the flow rate has dual effects on the photocatalytic reaction of these VOCs. As previously described, the adsorption of pollutants on the surface of the optimized TNP is also an important factor which can be correlated with the flow rate. The TNP possesses a high surface area with porosity, which makes it superior to the Degussa P 25 in terms of adsorption capacity [25]. The adsorption of ethylene, propylene, and toluene on the optimized TNP is also different. It has been observed that the adsorption on ethylene/propylene is in the form of a monolayer. However, in the case of toluene, the adsorption appears to be very high due to the multilayers which make it difficult to initiate the reaction as shown in the reaction trend. The reaction with toluene might also be slow due to the formation of polymeric substances observed at 3670 cm^{-1} which are associated with OH groups as shown in Fig. 9.

3.5.2. Concentration effect

The second important factor that should be discussed is the feed concentration of the VOCs. A catalyst saturation and adsorption competition phenomenon is usually observed at the higher feed concentrations of the pollutants [18]. This effect is shown in Fig. 10 pertaining to ethylene, propylene, and toluene. Fig. 10a shows that the increased concentration of ethylene led to a gradual decrease in the conversion rate when the optimized TNP was used. However, the catalyst has the ability to work even with higher concentration of 500 ppm but the result is lower conversion rate.

In the case of propylene (Fig. 10b), the optimized TNP has shown a good performance (90% conversion) due to the low concentration and monolayer adsorption. As the concentration increased, a gradual decrease and deactivation was observed, which might be due to the formation of deactivating byproducts.

Finally, the optimized TNP in Fig. 10c shows a good and stable conversion for 100 ppm of toluene, but when the concentration is increased from 100 to 200 ppm, the conversion curve shows an overall decrease. A further increase in concentration to 500 ppm significantly decreased the conversion to very low levels, likely because of surface flooding.

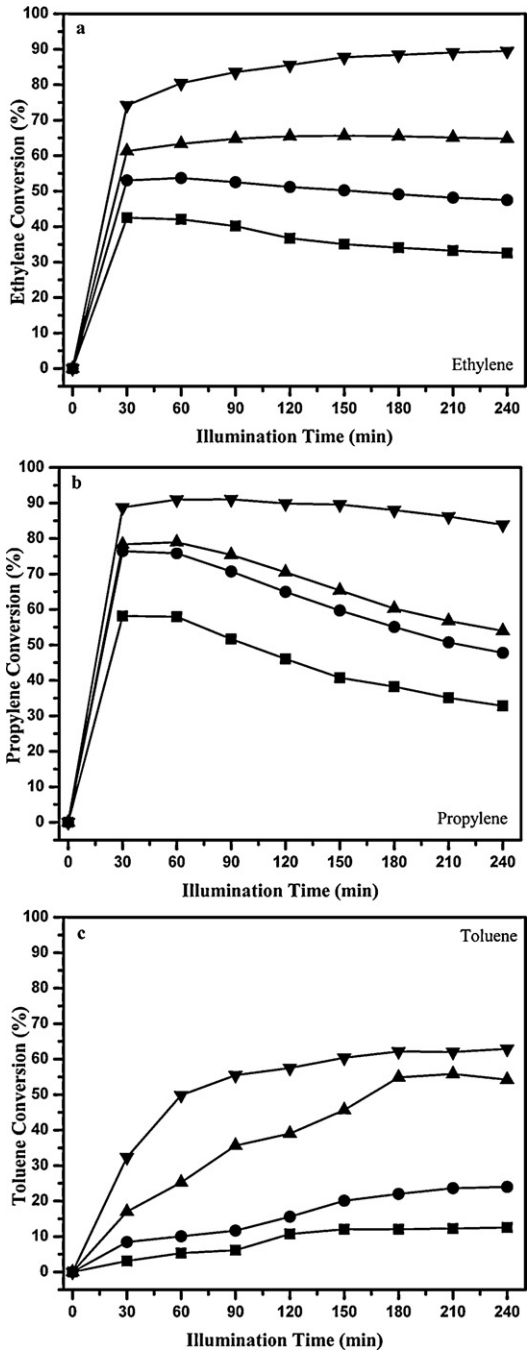

Fig. 10. Effect of concentration (ppm) on the photocatalytic activity of the optimized TNP for VOC abatement (a) ethylene, (b) propylene, (c) toluene, fed at 100 mL/min flow rate, at room temperature, over 1 g of TNP (400 °C/3 h): (▼) 100 ppm; (▲) 200 ppm; (●) 300 ppm; (■) 500 ppm.

3.5.3. Catalyst weight effect

The third important factor that affects the photocatalytic activity of the optimized TNP is the catalyst weight that is available in the reactor, as shown in Fig. 11. Fig. 11a shows the effect of the optimized TNP weight on the conversion of ethylene. Catalyst was dispersed on the bottom surface of the reactor and a gradual increase in the catalyst weight resulted in the area available in the reactor becoming covered. A further increase in the catalyst weight led to the formation of the multilayers which were not accessible to the reaction. As the catalyst weight increased from 1 to 2 g, there was a gradual increase in the conversion, but a further increase till 3 g led to a decrease in the conversion. This can also be explained by the fact that the optimized TNP has a higher surface area, with porosity, which offers more surface due to the increased weight which caused the higher adsorption and consequently the higher conversion. A further increase in weight made the internal mass transfer and light penetration limitations become more and more important. These limitations entailed that the increase in the available catalyst mass did not actually lead to an increase in terms of increased ethylene conversion.

However, the increase in catalyst weight was particularly beneficial for the propylene conversion as shown in Fig. 11b. The conversion increased whenever the catalyst weight was increased from 1.5 to 3 g, but no further conversion increase was expected. Moreover, it showed stability for 6 h of illumination time, because a sufficient surface area of the TNP was available for the increased adsorption of propylene as well as byproducts compared to ethylene. The propylene trend for 1 g instead showed deactivation due to the fact that an insufficient catalyst surface was available for adsorption of byproducts. It should be expected that deactivation could play a role and also becomes evident for the higher catalyst amounts. However, this can happen for higher operating times than 6 h.

Similar trends to those of propylene were also observed for toluene, as shown in Fig. 11c. An increase in weight from 1.5 to 3 g showed a dramatic increase in conversion even from the initial illumination time of 30 min. 3 g of the catalysts resulted in an optimized long term conversion which might be due to the fact that more surface was available for the adsorption and reaction.

3.5.4. Temperature effect

Another factor that affects VOC photocatalytic abatement is the operating temperature, as shown in Fig. 12. The main objective of this study was to use the optimized TNP efficiently at room temperature. However, a small increase in temperature to 35 °C showed an increase in the ethylene conversion. Conversely, when a higher temperature of 80 °C, was reached, a decrease was observed (Fig. 12a). A similar trend was observed for propylene and toluene (Fig. 12b and c), and the highest conversion was shown at 40 °C. This is due to the best compromise between the increase in reaction kinetics and the decrease in adsorption entailed by the temperature rise.

3.6. Optimized TNP vs. Degussa P 25 for VOC abatement

Fig. 13 shows a comparison of the optimized TNP and the Degussa P 25 catalysts for ethylene, propylene, and toluene at room temperature.

In all three cases of VOC photodegradation for mineralization, the optimized TNP has shown a superior activity and stability than that of Degussa P 25. TNP has small nanoparticles with a higher surface area and porosity than the non-porous Degussa P 25 [25]. It is also possible that the TNP material has a more amenable anatase-to-rutile ratio (80:20) compared to Degussa P 25. Anatase phase based TiO_2 is usually better than rutile for photocatalytic reactions due to its better adsorption affinity [33]. This difference is due to the

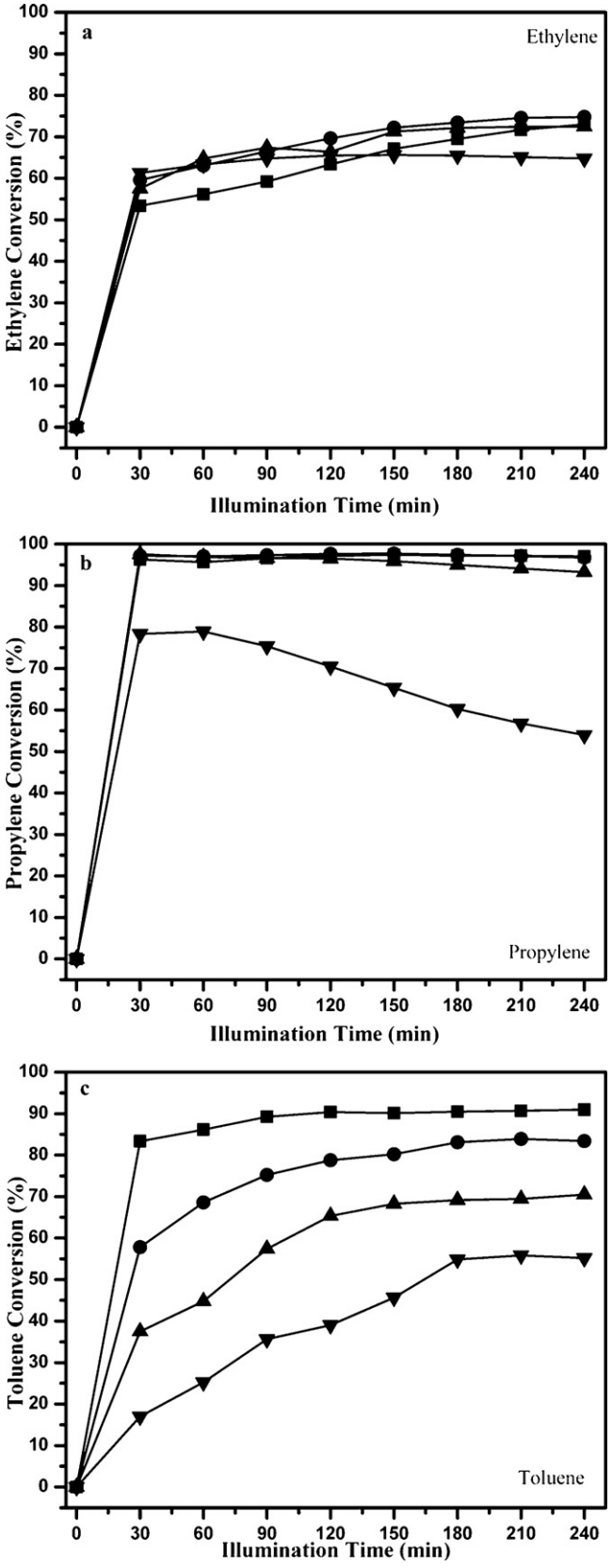

Fig. 11. Effect of catalyst weight on the photocatalytic activity of the optimized TNP for VOC abatement (a) ethylene, (b) propylene, (c) toluene, fed at 200 ppm within a 100 mL/min flow rate at room temperature: (▼) 1 g TNP (400 °C/3 h); (▲) 1.5 g TNP (400 °C/3 h); (●) 2 g TNP (400 °C/3 h); (■) 3 g TNP (400 °C/3 h).

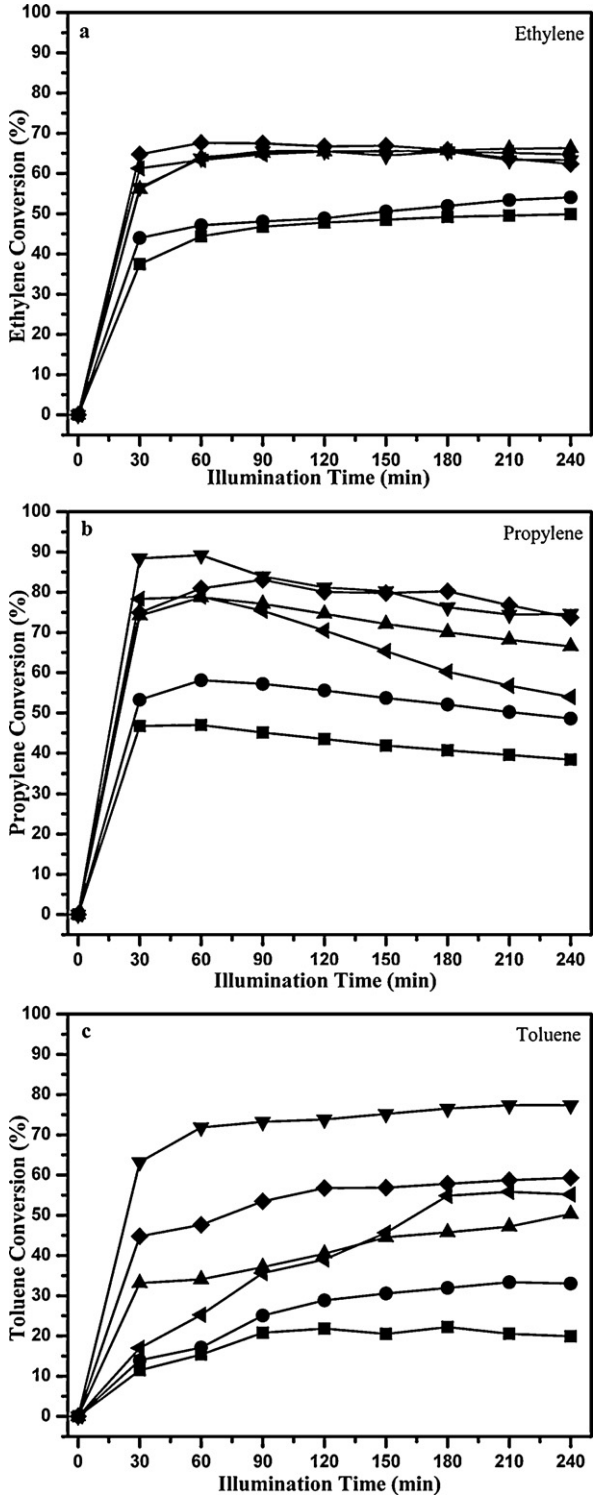

Fig. 12. Effect of reaction temperature on photocatalytic activity of the optimized TNP for VOC abatement (a) ethylene, (b) propylene, (c) toluene, fed at 200 ppm, in a 100 mL/min flow rate, over 1 g TNP (400 °C/3 h): (◄) room temperature/30 °C; (♦) 35 °C; (▼) 40 °C; (▲) 50 °C; (●) 60 °C; (■) 80 °C.

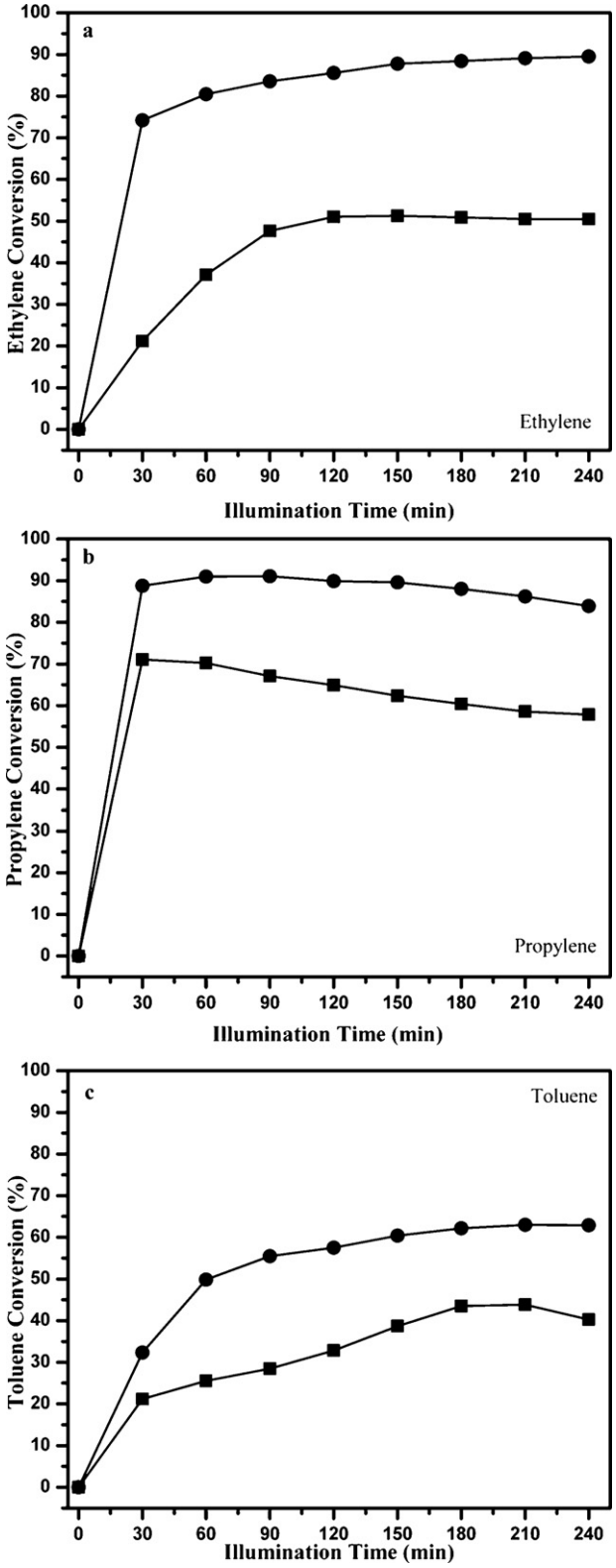

Fig. 13. Comparison of the optimized TNP vs. Degussa P 25 for VOC abatement (a) ethylene, (b) propylene, (c) toluene, fed at 100 ppm, in a 100 mL/min flow rate, over 1 g of catalyst at room temperature: (●) TNP (400 °C/3 h); (■) Degussa P 25.

structural difference of anatase and rutile. Both anatase and rutile have tetragonal structures with $[TiO_6]^{2-}$ octahedra, which share edges and corners in different manners but maintain the overall TiO_2 stoichiometry. Four edges of the $[TiO_6]^{2-}$ octahedra in anatase, are shared, thus forming a zigzag chain of octahedra that are linked to each other through shared edges, but as far as rutile is concerned, two opposite edges of each $[TiO_6]^{2-}$ octahedra are shared to form

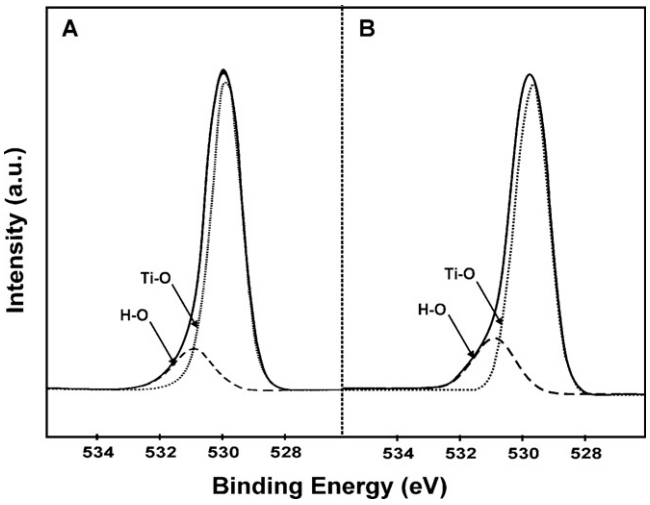

Fig. 14. XPS analysis showing the difference between the Degussa P 25 (a) and the optimized TNP (b) materials in terms of O 1s presence.

a linear chain and these chains are further linked to each other by the corner oxygen atoms. For this reason, the surface properties of anatase and rutile exhibit considerable differences. Rutile is characterized by a surface where the dissociation of the adsorbed organic molecules takes place much more easily than on anatase. These essential differences in the surface chemistry of the two TiO_2 phases result in differences in photocatalytic properties since the photocatalysis reactions mainly take place on the surface of the catalyst rather than in the bulk. Rutile titania has a much lower specific surface area than that of anatase. As the specific surface area of the catalyst increases, it can adsorb more VOCs. Moreover, anatase exhibits lower electron–hole recombination rates than rutile due to its 10-fold greater electron trapping rate. Therefore, the mixed optimized TNP phase with a high surface area is the main characteristic which makes it superior to Degussa P 25.

Moreover, TNP has more surface OH groups than Degussa P 25, as was observed using FT-IR [25]. However, further confirmation is here provided from the results of the direct XPS measurements. XPS analysis is extensively used to evaluate hydroxyl groups and the evolution of the valence state of titanium on TiO_2 surfaces [8,46]. Fig. 14 shows the oxygen O 1s XPS spectra and the deconvolution results of the optimized TNP and Degussa P 25 from a quantitative

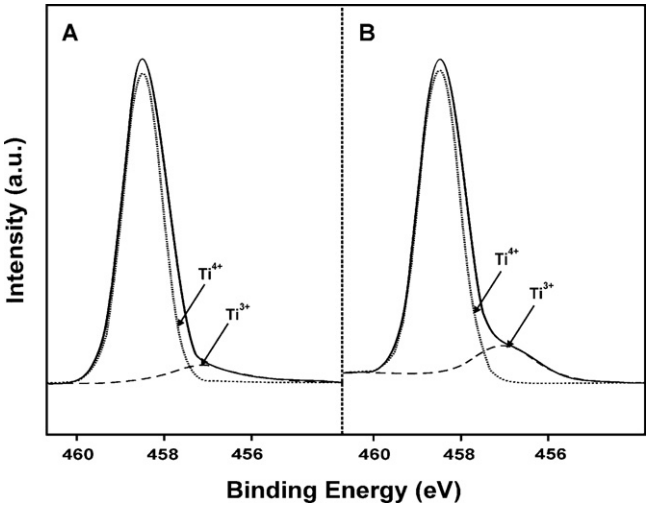

Fig. 15. XPS analysis showing the difference between the Degussa P 25 (a) and the optimized TNP (b) materials in terms of Ti species presence.

Table 3
Atomic concentrations (%) of TiO_2 by using XPS.

Catalyst	O 1s	Ti 2p	Ti–O	O–H	Ti^{3+}	Ti^{4+}
Degussa P 25	69.87	30.13	86.69	13.31	8.93	91.07
TNP 400 °C 3 h	70.57	29.43	82.05	17.95	17.77	82.23

point of view. The O 1s spectrum displayed peaks at 529.6 eV associated to Ti–O bonds in TiO_2, at 530.8 eV which correspond to the hydroxyl Ti–OH [8,42,47] that can be observed in the XPS spectra in Fig. 14 (a: Degussa P 25; b: optimized TNP). The optimized TNP clearly showed more OH groups on the surface than Degussa P 25. The quantitative results are shown in Table 3. The mass fraction of O 1s and the hydroxyl groups of the two samples were calculated from the results of the curve fitting of the XPS spectra for the O 1s region. The O 1s values for the optimized TNP and Degussa P 25 were 70.57, 69.87%, respectively, and are similar. However, the O–H species for the optimized TNP (17.95%) and Degussa P 25 (13.31%) are different. The higher OH groups on the surface of the optimized TNP could also play a major role than Degussa P 25 due to its superior photocatalytic activity in VOC abatement.

Fig. 15 shows the Ti peaks which are at binding energies of 456.7 eV (Ti^{3+}) and 458.5 eV (Ti^{4+}) [42] for Degussa P 25 (a) and the optimized TNP (b). It is very clear that the optimized TNP has more Ti^{3+} species than Degussa P 25. After proper calculation through curve fitting, Table 3 shows that the optimized TNP and the Degussa P 25 catalysts have similar Ti_{2P} values but different Ti species. The optimized TNP material has 17.77% Ti^{3+} while Degussa P 25 only shows 8.93%. The Ti^{3+} species are responsible for oxygen photadsorption which results in the formation of O_{ads}^{-}, and which, together with the OH radical, is essential for photocatalytic oxidation [41,48]. The presence of surface Ti^{3+} causes distinct differences in the nature of the chemical bonding between the adsorbed molecule and the substrate surface. These results correlate with Eqs. (7) and (8) in mechanism Section 3.4.

4. Conclusions

A new TNP material has been successfully synthesized in a vortex reactor using the sol–gel process with controlled operating parameters. It has been optimized by controlling the calcination temperature and time. Small nanoparticles have been obtained with little porosity and a large surface area, which is mainly constituted by anatase with small rutile amounts (mixed phase). These nanoparticles characterized by confined band gap energy and high surface OH group concentrations. The optimized TNP sample (400 °C/3 h) has shown a better photocatalytic performance towards ethylene oxidation than other samples at ambient temperature in an ad hoc designed Pyrex glass photocatalytic reactor due to its superior structural and chemical–physical characteristics.

The optimized TNP has been applied to the abatement of three different VOCs (ethylene, propylene, and toluene) in order to investigate its potential for practical applications. The effect of different factors, including adsorption, flow rate, concentration, catalyst weight, and reaction temperature has shown a close correlation between the performance and the nature of the optimized TNP. The developed material has shown a superior catalytic performance of VOCs than that of Degussa P 25 TiO_2. The presence of an anatase–rutile mixed phase, the high specific surface area with good porosity, and the increase in Ti^{3+} species might induce increased adsorption of the VOC pollutants and water with the generation of OH groups (oxidizing agent) on the surface of the TNP catalyst, which results in a higher photocatalytic activity. The superior catalytic performance of the optimized TNP compared to the best commercial Degussa P 25 TiO_2 for VOC application makes it promising for future research and further applications.

Acknowledgements

M. Hussain is grateful to the Regione Piemonte and the Politecnico di Torino, Italy for his post-doctoral fellowship grant.

References

[1] P. Avila, A. Bahamonde, J. Blanco, B. Sanchez, A.I. Cardona, M. Romero, Gas-phase photo-assisted mineralization of volatile organic compounds by monolithic titania catalysts, Appl. Catal. B: Environ. 17 (1998) 75–88.
[2] S. Wang, H.M. Ang, M.O. Tade, Volatile organic compounds in indoor environment and photocatalytic oxidation: state of the art, Environ. Int. 33 (2007) 694–705.
[3] K. De Witte, V. Meynen, M. Mertens, O.I. Lebedev, G. Van Tendeloo, A. Sepulveda-Escribano, F. Rodriguez-Reinoso, E.F. Vansant, P. Cool, Multi-step loading of titania on mesoporous silica: influence of the morphology and the porosity on the catalytic degradation of aqueous pollutants and VOCs, Appl. Catal. B: Environ. 84 (2008) 125–132.
[4] W.-K. Jo, K.-H. Park, Heterogeneous photocatalysis of aromatic and chlorinated volatile organic compounds (VOCs) for non-occupational indoor air application, Chemosphere 57 (2004) 555–565.
[5] R.M. Alberici, W.F. Jardim, Photocatalytic destruction of VOCs in the gas-phase using titanium dioxide, Appl. Catal. B: Environ. 14 (1997) 55–68.
[6] D.S. Tsoukleris, T. Maggos, C. Vassilakos, P. Falaras, Photocatalytic degradation of volatile organics on TiO_2 embedded glass spherules, Catal. Today 129 (2007) 96–101.
[7] W.-K. Jo, J.-H. Park, H.-D. Chun, Photocatalytic destruction of VOCs for in-vehicle air cleaning, J. Photochem. Photobiol. A: Chem. 148 (2002) 109–119.
[8] F.-L. Toma, G. Bertrand, S. Begin, C. Meunier, O. Barres, D. Klein, C. Coddet, Microstructure and environmental functionalities of TiO_2-supported photocatalysts obtained by suspension plasma spraying, Appl. Catal. B: Environ. 68 (2006) 74–84.
[9] H. Yu, K. Zhang, C. Rossi, Theoretical study on photocatalytic oxidation of VOCs using nano-TiO_2 photocatalyst, J. Photochem. Photobiol. A: Chem. 188 (2007) 65–73.
[10] M.B. Ray, Photodegradation of the volatile organic compounds in the gas phase: a review, Dev. Chem. Eng. Mineral Process. 8 (2000) 405–439.
[11] S. Kumar, A.G. Fedorov, J.L. Gole, Photodegradation of ethylene using visible light responsive surfaces prepared from titania nanoparticle slurries, Appl. Catal. B: Environ. 57 (2005) 93–107.
[12] F. Benoit-Marquié, U. Wilkenhöner, V. Simon, A.M. Braun, E. Oliveros, M.T. Maurette, VOC photodegradation at the gas–solid interface of a TiO_2 photocatalyst. Part I. 1-Butanol and 1-butylamine, J. Photochem. Photobiol. A: Chem. 132 (2000) 225–232.
[13] J. Biomorgi, E. Oliveros, Y. Coppel, F. Benoit-Marquié, M.T. Maurette, Effect of V-UV-radiation on VOCs-saturated zeolites, J. Photochem. Photobiol. A: Chem. 214 (2010) 194–202.
[14] G. Martra, S. Coluccia, L. Marchese, V. Augugliaro, V. Loddo, L. Palmisano, M. Schiavello, The role of H_2O in the photocatalytic oxidation of toluene in vapour phase on anatase TiO_2 catalyst: a FTIR study, Catal. Today 53 (1999) 695–702.
[15] D.S. Muggli, L. Ding, Photocatalytic performance of sulfated TiO_2 and Degussa P-25 TiO_2 during oxidation of organics, Appl. Catal. B: Environ. 32 (2001) 181–194.
[16] Z. Pengyi, L. Fuyan, Y. Gang, C. Qing, Z. Wanpeng, A comparative study on decomposition of gaseous toluene by O_3/UV, TiO_2/UV and O_3/TiO_2/UV, J. Photochem. Photobiol. A: Chem. 156 (2003) 189–194.
[17] C.H. Ao, S.C. Lee, Combination effect of activated carbon with TiO_2 for the photodegradation of binary pollutants at typical indoor air level, J. Photochem. Photobiol. A: Chem. 161 (2004) 131–140.
[18] M. Sleiman, P. Conchon, C. Ferronato, J.-M. Chovelon, Photocatalytic oxidation of toluene at indoor air levels (ppbv): towards a better assessment of conversion, reaction intermediates and mineralization, Appl. Catal. B: Environ. 86 (2009) 159–165.
[19] M.C. Blount, J.L. Falconer, Steady-state surface species during toluene photocatalysis, Appl. Catal. B: Environ. 39 (2002) 39–50.
[20] F. Fresno, M.D. Hernandez-Alonso, D. Tudela, J.M. Coronado, J. Soria, Photocatalytic degradation of toluene over doped and coupled (Ti,M)O_2 (M = Sn or Zr) nanocrystalline oxides: influence of the heteroatom distribution on deactivation, Appl. Catal. B: Environ. 84 (2008) 598–606.
[21] L. Zou, Y. Luo, M. Hooper, E. Hu, Removal of VOCs by photocatalysis process using adsorption enhanced TiO_2–SiO_2 catalyst, Chem. Eng. Process. 45 (2006) 959–964.
[22] G.-M. Zuo, Z.-X. Cheng, H. Chen, G.-W. Li, T. Miao, Study on photocatalytic degradation of several volatile organic compounds, J. Hazard. Mater. B 128 (2006) 158–163.
[23] P.-A. Deveau, F. Arsac, P.-X. Thivel, C. Ferronato, F. Delpech, J.-M. Chovelon, P. Kaluzny, C. Monnet, Different methods in TiO_2 photodegradation mechanism studies: gaseous and TiO_2-adsorbed phases, J. Hazard. Mater. 144 (2007) 692–697.
[24] V. Augugliaro, S. Coluccia, V. Loddo, L. Marchese, G. Martra, L. Palmisano, M. Schiavello, Photocatalytic oxidation of gaseous toluene on anatase TiO_2 catalyst: mechanistic aspects and FT-IR investigation, Appl. Catal. B: Environ. 20 (1999) 15–27.
[25] M. Hussain, R. Ceccarelli, D.L. Marchisio, D. Fino, N. Russo, F. Geobaldo, Synthesis, characterization, and photocatalytic application of novel TiO_2 nanoparticles, Chem. Eng. J. 157 (2010) 45–51.
[26] D.S. Bhatkhande, V.G. Pangarkar, A.A.C.M. Beenackers, Photocatalytic degradation for environmental applications—a review, J. Chem. Technol. Biotechnol. 77 (2001) 102–116.
[27] J. Peral, X. Domenech, D.F. Ollis, Heterogeneous photocatalysis for purification, decontamination and deodorization of air, J. Chem. Technol. Biotechnol. 70 (1997) 117–140.
[28] A. Mills, S.L. Hunte, An overview of semiconductor photocatalysis, J. Photochem. Photobiol. A: Chem. 108 (1997) 1–35.
[29] D.R. Park, J. Zhang, K. Ikeue, H. Yamashita, M. Anpo, Photocatalytic oxidation of ethylene to CO_2 and H_2O on ultrafine powdered TiO_2 photocatalysts in the presence of O_2 and H_2O, J. Catal. 185 (1999) 114–119.
[30] A. Fujishima, K. Hashimoto, T. Watanabe, TiO_2 Photocatalysis: Fundamentals and Applications, English ed., BKC Inc., Tokyo, 1999.
[31] A. Fujishima, T.N. Rao, D.A. Tryk, Titanium dioxide photocatalysis, J. Photochem. Photobiol. C: Photochem. Rev. 1 (2000) 1–21.
[32] A. Fujishima, X. Zhang, Titanium dioxide photocatalysis: present situation and future approaches, C. R. Chim. 9 (2006) 750–760.
[33] P. Periyat, K.V. Baiju, P. Mukundan, P.K. Pillai, K.G.K. Warrier, High temperature stable mesoporous anatase TiO_2 photocatalyst achieved by silica addition, Appl. Catal. A: Gen. 349 (2008) 13–19.
[34] S.S. Watson, D. Beydoun, J.A. Scott, R. Amal, The effect of preparation method on the photoactivity of crystalline titanium dioxide particles, Chem. Eng. J. 95 (2003) 213–220.
[35] R.R. Bacsa, J. Kiwi, Effect of rutile phase on the photocatalytic properties of nanocrystalline titania during the degradation of p-coumaric acid, Appl. Catal. B: Environ. 16 (1998) 19–29.
[36] A. Testino, I.R. Bellobono, V. Buscaglia, C. Canevali, M. D'Arienzo, S. Polizzi, R. Scotti, F. Morazzoni, Optimizing the photocatalytic properties of hydrothermal TiO_2 by the control of phase composition and particle morphology. A systematic approach, J. Am. Chem. Soc. 129 (2007) 3564–3575.
[37] C. Su, B.Y. Hong, C.M. Tseng, Solgel preparation and photocatalysis of titanium dioxide, Catal. Today 96 (2006) 119–126.
[38] K. Porkodi, S.D. Arokiamary, Synthesis and spectroscopic characterization of nanostructured anatase titania: a photocatalyst, Mater. Charact. 58 (2007) 495–503.
[39] K. Mogyorosi, I. Dekany, J.H. Fendler, Preparation and characterization of clay mineral intercalated titanium dioxide nanoparticles, Langmuir 19 (2003) 2938–2946.
[40] G. Tian, H. Fu, L. Jing, C. Tian, Synthesis and photocatalytic activity of stable nanocrystalline TiO_2 with crystallinity and large surface area, J. Hazard. Mater. 161 (2009) 1122–1130.
[41] Z. Xu, J. Shang, C. Liu, C. Kang, H. Guo, Y. Du, The preparation and characterization of TiO_2 ultrafine particles, Mater. Sci. Eng. B 56 (1999) 211–214.
[42] P.M. Kumar, S. Badrinarayanan, M. Sastry, Nanocrystalline TiO_2 studied by optical, FTIR and X-ray photoelectron spectroscopy: correlation to presence of surface states, Thin Solid Films 358 (2000) 122–130.
[43] F. Arsac, D. Bianchi, J.M. Chovelon, P. Conchon, C. Ferronato, A. Lair, M. Sleiman, Photocatalytic degradation of organic pollutants in water and in air. An analytical approach, Mater. Sci. Eng. C 28 (2008) 722–725.
[44] K. Yogo, M. Ishikawa, Recent progress in environmental catalytic technology, Catal. Surv. Jpn. 4 (2000) 83–90.
[45] J.-M. Herrmann, C. Duchamp, M. Karkmaz, Bui Thu Hoai, H. Lachheb, E. Puzenat, C. Guillard, Environmental green chemistry as defined by photocatalysis, J. Hazard. Mater. 146 (2007) 624–629.
[46] G. Colon, M.C. Hidalgo, G. Munuera, I. Ferino, M.G. Cutrufello, J.A. Navıo, Structural and surface approach to the enhanced photocatalytic activity of sulfated TiO_2 photocatalyst, Appl. Catal. B: Environ. 63 (2006) 45–49.
[47] Y.D. Hou, X.C. Wang, L. Wu, X.F. Chen, Z.X. Ding, X.X. Wang, X.Z. Fu, N-doped SiO_2/TiO_2 mesoporous nanoparticles with enhanced photocatalytic activity under visible-light irradiation, Chemosphere 72 (2008) 414–421.
[48] X. Fang, Z. Zhang, Q. Chen, H. Ji, X. Gao, Dependence of nitrogen doping on TiO_2 precursor annealed under NH_3 flow, J. Solid State Chem. 180 (2007) 1325–1332.